International Journal of Engineering Inventions
e-ISSN: 2278-7461, p-ISSN: 2319-6491
Volume 14, Issue 4 [April. 2025] PP: 35-43

The structure, properties and antibacterial activity of manganese-doped zinc oxide (5 mol%) nanoparticles against gram-positive and gram-negative bacteria

JanmejayYadav[1],Vikram Singh[2], RamKripal[3*],Rajesh Kumar Yadav[4] and UrvashiSrivatava[5]

[1]*Department of Physics, Nehru Gram Bharati (Deemed to be University), Jamunipur, Prayagraj,India(Orcid ID: https://orcid.org/0009-0004-8938-983X)*
[2]*Department of Physics, Nehru Gram Bharati (Deemed to be University), Jamunipur, Prayagraj, India (Orcid ID: https://orcid.org/0000-0003-3813-586X)*
[3]*EPR Laboratory, Department of Physics, University of Allahabad, Prayagraj, India (Orcid ID: https://orcid.org/0000-0002-3483-8704)*
[4]*Department of Physics, CMP Degree College, University of Allahabad,Prayagraj,India(Orcid ID: https://orcid.org/0000-0002-7362-6034)*
[5]*Department of Home Science,Prof.Rajendra Singh (RajjuBhaiya) University Prayagraj, India(Orcid ID: https://orcid.org/0000-0002-0779-155X),*

Abstract
The defined size of manganese-doped zinc oxide (5 mol%) nanocrystalline powders formed using an aqueous chemical process that doesn't involve a coating agent is the main objective of this research. Dissimilar calcination temperatures were used to discern how the size of the ZnO nanoparticles was magnified. The optical features were examined using UV-vis spectroscopy in diffused reflectance (DR) mode. It exhibited a significant surge in reflectivity at 370 nm and a projecting reflective feature at 420 nm at 500◦C calcination temperature. Conferring to Scherrer's formula and W-H analysis, as the calcination temperature increased, the typical crystallite size of ZnO nanoparticles (5 mol%) increased. Transmission electron microscopy (TEM) and scanning electron microscopy (SEM) were used to examine morphology and elemental constitution. Both ZnO and Mn-doped zinc oxide nanoparticles revealed grander antibacterial activity against gram positive (Staphylococus aureus) and gram negative bacteria (Shigellaflexneri, Salmonella typhiand E. coli).

Keywords*—Mn-doped nanoparticles, zinc oxide, Scherrer's equation, Antibacterial activity, nanoparticles*

Date of Submission: 05-04-2025 Date of acceptance: 16-04-2025

I. INTRODUCTION

In contrast to their bulk counterparts, semiconductor nanoparticles have concerned a lot of consideration lately due to their distinguishing optical characteristics, enormous surface-to-volume ratio, and incomparable electrical assets [1]. Some of the special features of nanoparticles may be ascribed to their high surface to volume ratio. One significant type of semiconductors are transition metal oxides [2–5]. Zinc oxide (ZnO), a exclusive electrical and photonic wurtzite n-type semiconductor amid other semiconducting oxides, has a high exciting binding energy (60 meV) at ambient temperature and a direct band gap of 3.37 eV [6–10]. ZnO's strong exciton requisite energy would enable excitonic transitions even at ambient temperature, hypothetically leading to a reduced threshold voltage for laser emanation and high radiate recombination adeptness for impulsive emanation [11, 12]. ZnO is used in mechanical actuators and piezoelectric sensors because of its in elevation piezoelectric and pyroelectric competences, which are caused by wurtzite's lack of center of symmetry and a significant electromechanical coupling [13]. Due to its comparable qualities to GaN, ZnO is a promising choice for optoelectronic applications in the short wavelength range (green, blue, and ultraviolet), information storage, and sensors [14, 15]. For a number of uses, counting solar cells, gas sensors, photodetectors, photocatalysts, and nanogenerators, ZnO nanoparticles offer interesting options [16–18]. The optical and electrical characteristics of ZnO nanoparticles, which are formed using a variability of chemical and physical methods such as vapour condensation, hydrothermal method, solution ignition method, sol–gel method, etc., have been the focus of several recent studies. The majority of these methods have not been extensively useful on a broad scale, however, because of their affordability and ease of use.. One of the greatest practices for producing materials with controlled nanostructures, high purity, and necessary surface features is the chemical route approach [19, 20]. These synthesis approaches are appealing for a number of reasons, they can be effortlessly scaled up due to their low cost and low toxicity; they can be united with well-established silicon technologies because they don't require metal catalysts; and they grow at a relatively low temperature, making them compatible with organic substrates.

Furthermore, a number of factors may be adjusted to efficiently regulate the end products' morphologies and physical characteristics. Nanoparticles were created using a straightforward aqueous chemical process with well regulated conditions and no capping agent.

The average crystallite size of ZnO nanoparticles as determined by powder X-ray diffraction (XRD) peak broadening and direct AFM measurements is compared.

The Williamson–Hall (W-H) technique has also been used to assess the average crystallite size and strain related to ZnO samples as a result of lattice deformation.

II. MATERIAL PROCESSING AND EXPERIMENTAL PROCEDURE OF PREPARATION OF MANGANESE DOPED ZINC OXIDE NANOCRYSTALLINE POWDER

2.1. Synthesis of ZnO and Mn-doped ZnO (5 mol%) nanoparticles

2.1.1Materials

Zinc acetate dihydrate [Zn $CH_3COO)_2\cdot 2H_2O$], Manganese acetate (98%), NaOH (99%)), H_2SO_4 (95%-97%), Ethanol (absolute), commercial ZnO (C-ZnO, 99%). All of the chemical reagents utilized in the experiment to produce zinc oxide and manganese-doped zinc oxide (5 mol%) nanoparticles were analytical grade [Merck with 99% purity] and didn't require any additional purification.

2.1.2. Preparation

Different concentrations of an ethanolic manganese acetate solution were combined with 75 mM of ethanolic zinc acetate solution to create the catalyst. To decrease the volume of the solution and raise the concentration of the metal ions, the combined solutions were heated to 75 °C for 45 minutes. They were then allowed to cool to room temperature. 0.3 M of NaOH solution was then added to the combined solution with steady stirring (150 rpm) until pH 8.3 was attained. For two hours, the new colorless solution was maintained at 67 °C in a water bath. After an hour in the water bath, it was seen that the solution began to precipitate. The colloidal solution was centrifuged for 20 minutes at 4000 rpm after being allowed to cool to room temperature for four hours. The resulting precipitate was washed with ethanol, sonicated (30 min), and centrifuged (4000 rpm). The above procedure was repeated five times to remove unreacted ions. The separated precipitate was dried overnight at 110°C. The catalyst was ground and then calcined under compressed air at 650ºC for 3.5h in the tubular furnace. Ultimately, after three hours of calcination at 150, 300, and 500 °C in a muffle furnace, nanocrystalline ZnO powders with a milky white hue were produced. Undoped ZnO was synthesized with a similar procedure except for the addition of manganese acetate.

2.2. Characterizations

ZnO nanoparticle powder X-ray diffraction data were collected by the Rigaku X Ray Diffractometer (Model: Smart Lab). With the help of three-kilogram Micro Universal Testing Machine (Micro UTM) for Tensile Stage Module of Scanning Electron Microscopy (SEM) Model: EVO MA 5 Micro Test 5000W: Using a 5000N load cell, the elemental compositions and morphology were examined. Scanning electron microscopy (SEM) and transmission electron microscopy (TEM) examinations demonstrated the particles' size and shape. The disc diffusion examination was used to evaluate the antibacterial activity of ZnO and Mn doped ZnO NPs against gram positive *Staphylococcus aureus* bacteria as well as gram negative *Shigellaflexneri*, *E. coli*, and *Salmonella typhi* bacteria. The related activity indexes are reported by them.

III. RESULTS AND DISCUSSION

3.1 X-ray diffraction analysis of ZnO Mn-doped ZnO (5 mol%) nanoparticles

Figure 1 (a, b) illustrates how various calcination temperatures affect ZnO and Mn-doped ZnO nanoparticles (5 mol%). At temperatures higher than 150 °C, all of the peaks were sharper, confirming the crystal formation at higher temperatures during calcination. Figure 1 makes it evident that no other phase of ZnO evolved than the hexagonal phase. The standard ZnO pattern was compared with the recorded X-ray diffraction patterns. When compared to lower calcination temperatures, ZnO nanoparticles calcined at higher temperatures change at peak positions (1 0 0), (0 0 1), and (1 0 1) towards the lower Bragg's angle. The ZnO nanoparticles' crystallite size was ascertained by using Scherrer's equation to the X-ray line broadening technique:

$$D = \frac{K\lambda}{\beta_{hkl}\cos\theta} \qquad (1)$$

Where, D is the crystallite size, λ is the wavelength of the Cu Kα radiation (1.5406 ˚A), K is the form factor (0.9), β_{hkl} is the scattering angle, and FWHM is the full width at half maximum (FWHM) in radians. The ZnO nanoparticles' average crystallite size, as shown in Table 1, was calculated to be between 32 and 46 nm.

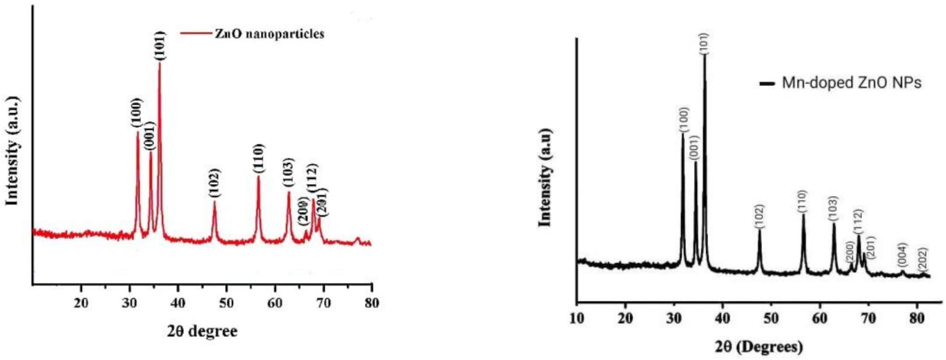

Fig. 1. Powder X-ray diffraction patterns of ZnO nanoparticles (a) The recorded XRD patterns for ZnO nanoparticles (b) The recorded XRD patterns for Mn-doped ZnO nanoparticles(5mol%).

The X-ray diffractometer (XRD) remains one of the most popular quantitative analytical tools for determining crystallite size. While the Scherrer formula is frequently used to predict nanostructural parameters, it only considers the effect of crystallite size on the XRD peak broadening and ignores the substantial intrinsic strain contribution [21]. Lattice strain and crystallite size quantify the size of coherently diffracting domains and the distribution of lattice constants from lattice dislocations, respectively [22, 23]. The point defect, grain boundary, and stacking faults are mainly responsible for the lattice strain due to doping, which may eventually lead to lattice expansion or lattice contraction in the nanocrystals [24]. The simplified W-H diagnostic tool assumes that the widening of Bragg's peaks is the total of peak broadening caused by induced strain and limited crystallite size [25].

Since the crystallite size of as-synthesised ZnO (as determined by XRD) is significantly bigger than the Bohr exciton radius of ZnO, which is 2.34 nm, the increase in band gap or blue shift in absorption may not be the result of the quantum confinement effect [26].

Table 1. Geometric properties of Mn-doped ZnO (5 mol%) nanoparticles at 150°C, 300°C, and 500°C are compared using Scherrer's formula and W-H analysis.

Calcination temperature (°C)	**Average crystallite size, D (nm)**		
	Scherrer's D (nm)	**Williamson–Hall analysis**	
		D (nm)	**E**
150	32	51	0.0080
300	43	70	0.0055
500	46	73	0.0046

3.2 Williamson–Hall analysis

Williamson-Hall X-ray line broadening analysis has been used to calculate the average size and strain of coherently diffracting domains. Crystal flaws generate strain-induced peak broadening and distortion, which were calculated using the following relationship:

$$\varepsilon = \frac{\beta_{hkl}}{4\tan\theta} \quad \textbf{(2)}$$

According to Zak et al. [27], Williamson and Hall suggested a modified Scherrer's formula, which was calculated using the following relation:

$$\beta_{hkl}\cos\theta = \frac{K\lambda}{D} + 4\varepsilon\sin\theta \quad \textbf{(3)}$$

Eq. (3) represents the linear plot of $\beta_{hkl}\cos\theta$ against 4 sinθ for the Mn-doped ZnO (5 mol%) calcined at 150 ˚C, 300 ˚C, and 500 ˚C temperatures shown in Fig. 2. The strain (ε) values obtained from the plots' slope are 0.0073, 0.0048, and 0.0058, respectively. Using the XRD-derived crystallite sizes (Scherrer's formula), which shows that tiny ε leads to large crystallite size, the results made sense; small grain size and small crystallite size were caused by large ε. The computations showed that the strain associated with the samples decreased as the crystallite size gradually increased as the calcination temperature increased from 150 °C to 500 °C, as shown in Table 1.

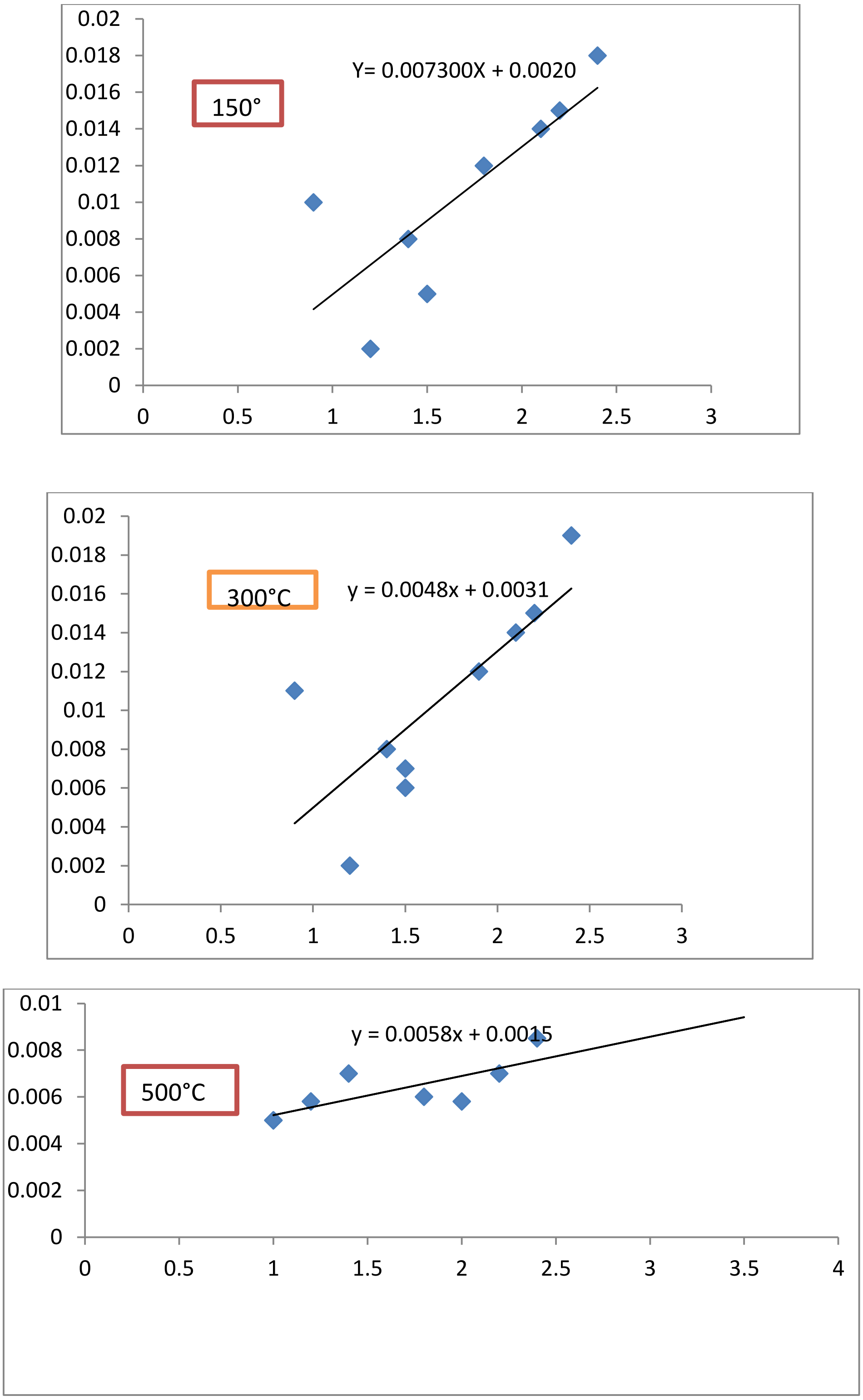

Fig. 2. Williamson–Hall analyses of Mn doped ZnO nanoparticles calcined at (a) 150°C, (b) 300 °C and (c) 500°C Temperatures assuming UDM plot.

3.3 Morphological evaluation

Scanning (SEM) and transmission (TEM) electron microscopy investigations confirmed the morphology and particle size. The 5 mol% sample's SEM image shows that the Mn doped ZnO powder is composed of 1-5μm aggregates of closely spaced particles that are less than 47 nm (Fig. 3). The TEM image of the same sample (Fig. 4) shows that, in fact, the Mn doped ZnO powder is composed of tiny particles, or quantum dots, with sizes smaller than three nanometers.

Because of their large surface area, these nanoparticles have a strong propensity to aggregate into much larger particles. Based on the SEM images, it was concluded that the Mn-doped ZnO (5 mol%) crystallite sizes were in the nanoscale range. The crystallite sizes grew from 32 nm to 46 nm when the calcination temperature increased from 150 °C to 500 °C. The nucleation rate of the particles increased with the calcination temperature. This is due to the fact that the greater supersaturation of the reaction products sped up the crystal core-forming process. In these circumstances, the reaction's regulating phase shifts from grain growth to the creation of the crystal nucleus.

It is definite that the fast formation of crystal nuclei is leading to a phenomenon called "nuclear-aggregation," which leads the crystal nuclei to coalesce, as the temperature rises. The rate of particle aggregation is one significant element affecting the final products' structure and form (crystallineness). It was discovered that bigger grain samples have inherently rougher edges due to their wider height variability (Z range). However, the morphologies were rather similar in each case. From the SEM observation, a similar conclusion may be drawn. The morphology was shown to be significantly influenced by the process parameters.

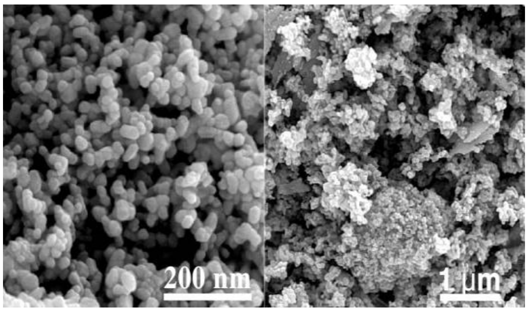

**Fig 3. SEM image of Mn doped ZnO nanopaticles (5 mol%)
(scale bar = 1 μm).**

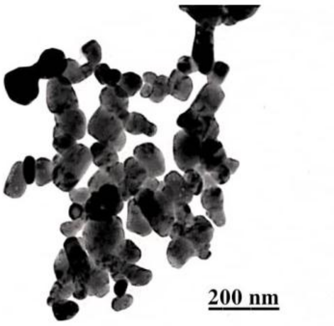

Fig.4.TEM image of Mn doped ZnO nanopaticles (5 mol%).

Table 1 lists the ZnO nanoparticles' geometric characteristics as established by Scherrer's formula and W-H analysis. Comparing the average crystallite size values derived from W–H analysis revealed that strain has a very slight impact on ZnO nanoparticle average crystallite size. The little variance in the average crystallite size as measured by Scherrer's formula and W-H analysis was caused by the disparity in averaging the particle size distribution.

3.4 Optical study: UV-vis analysis

The findings of a study on the effects of varying calcination temperatures on the optical properties of ZnO nanoparticles are shown in Figure 5. The diffused reflectance spectra of the 500°C-calcined sample showed a notable rise around 370 nm, and the material exhibited a high reflecting feature beyond roughly 450 nm. This was because photons that lacked the energy to interact with atoms or electrons were more likely to reflect back. It was demonstrated that the ZnO nanoparticles' capacity to absorb was significantly influenced by their particle sizes. The band gap energies were computed using the Kubelka-Munk function.

$$F(R) = \frac{(1 - R)^2}{2R}$$

Here, the absorption coefficient is equal to F(R) and R is the absolute value of the reflectance. Graphing was used to measure the direct band gap of ZnO

$$[F(R)\cdot h\nu]^{2} \text{ vs. } h\nu \text{ (eV).}$$

As the temperature rose from 150 °C to 500 °C, the obtained band gap energy (E_g) values were 3.15, 3.11, and 3.9 eV, respectively. The optical absorption edge considerably moved toward a longer wavelength in contrast to the observed band gap energy of bulk ZnO (E_g = 3.27 eV) [28]. Grain size may have increased at higher calcination temperatures, causing this shift.

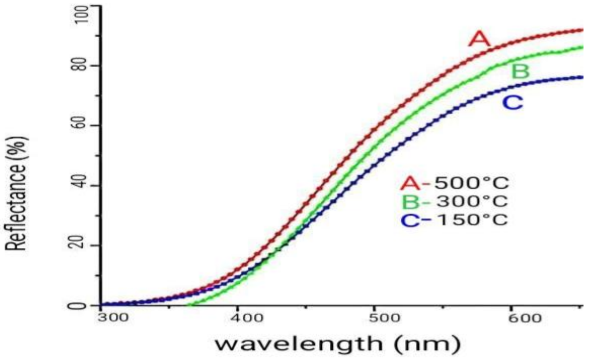

Fig. 5. Diffuse reflectance spectra of the ZnO nanoparticles calcined at 150 °C, 300 °C and 500 °C temperatures.

3.5 Antibacterial Activity

The antibacterial efficacy of ZnO and Mn doped ZnO NPs against gram negative *Salmonella typhi, Shigellaflexneri*and *E. coli* bacteria as well as gram positive *Staphylococcus aureus* bacteria was assessed using the disc diffusion technique. They report the related activity indexes. Figures 6 and 7 display the activity index for each catalyst as well as the average and standard deviation in the zones of inhibition. After a 24-hour incubation period, Mn-doped ZnO shows strong bactericidal activity measured in terms of zone of inhibition (mm). The antibacterial activity of Mn-doped ZnO against bacteria is superior to that of pure ZnO (Table 2).

Staphylococus aureus, Salmonella typhi, Shigellaflexneri, and *E. coli* growth might be inhibited by Mn-doped ZnO at mean concentrations of 21.4±1.02, 15.7±0.14, 20.5±1.01, and 16.9±1.13, respectively (Table 3). Mn-doped ZnO has increased activity because of the improved adherence of Mn atoms to the bacterial cell walls. Metal ions are known to attach to cell membranes by disrupting the thiol groups of proteins, rendering respiratory enzymes inactive. The increased electrostatic interactions between the NPs and the cell surface have also been proposed to cause a progressive change in the cell's shape, which increases permeability and leads to the accumulation of NPs in the cell's cytoplasm [29].

The accumulating NPs harm DNA by promoting lipid peroxidation and internal oxidative stress [30]. Thus, NPs' enhanced generation of ROS and accumulation, which commonly results in cell wall rupture and eventually cell death, can be used to explain why they have bactericidal effect [31].

Additionally, it has been suggested that the enhanced electrostatic interactions between the NPs and the cell surface gradually alter the shape of the cell, increasing permeability and causing NPs to accumulate in the cytoplasm of the cell [32]**.** By encouraging internal oxidative stress and lipid peroxidation, the accumulating NPs damage DNA [33]. Therefore, it is possible to explain why NPs have bactericidal activity by pointing to their increased production of reactive oxygen species (ROS) ROS and buildup, which frequently causes cell wall rupture and ultimately culminates in cell death. Ag-doped TiO_2 NPs have shown outstanding antibacterial action against *E. coli* [34]. Mn can be regarded as a significant metal dopant with potential antibacterial activity, and it can also be explored as a significant candidate material in future research, which will allow for the investigation of even larger percentages of metal ion doping. Pure and doped ZnO NPs were found to have strong antibacterial action against *Staphylococus aureus, Salmonella typhi, Shigellaflexneri, and E. coli bacteria.* This is because Ag ions have been demonstrated to significantly bind with thiol groups found in important bacterial enzymes, leading to their deactivation [35]. Mn-doped ZnO NPs can effectively inhibit the growth of four bacterial pathogens: *Shigellaflexneri*, *Salmonella typhi*, *E. coli*, and *Staphylococus aureus.* The increased activity of Mn-doped ZnO is due to the adherence effectiveness of Mn atoms to the bacterial cell walls. It is widely believed that metal ions bind to cell membranes by interacting with protein thiol groups, deactivating respiratory enzymes, and producing ROS [36]. The 5 mol% Mn doped ZnO exhibited the highest activity.

Table 2. The antimicrobial activity of ZnO with zone of inhibition.

Organism	**Zone of inhibition (mm)**					**Mean value ± SEM**	**Activity index**
	Concentration of ZnO in µg/ml						
	200	**400**	**600**	**800**	**1000**		
Salmonella typhi	14.5	16.3	17.5	19	20.5	14.6±0.04	0.7607
Shigellaflexneri	11	12.4	13.6	15	17.2	13.8±1.04	0.7534
Staphylococus aureus	12.5	14.5	15.5	18	21.2	16.3±0.13	0.7719
E.coli	9.5	11	13.5	14.8	16.5	13.1±1.10	0.6818

Table 3. The antimicrobial activity of ZnO (5 mol% Mn doped) with zone of inhibition.

Organism	**Zone of inhibition (mm)**					**Mean value ± SEM**	**Activity index**
	Concentration Mn-dopedof ZnO in µg/ml						
	200	**400**	**600**	**800**	**1000**		
Salmonella typhi	17.4	19.7	21.1	23.8	25.3	21.4±1.02	0.8701
Shigellaflexneri	12.2	15.7	15.8	16.7	18.3	15.7±0.14	0.8333
Staphylococus aureus	16.2	19.3	20.8	22	24.3	20.5±1.01	0.8000
E.coli	13.7	15.6	17.3	18.7	19.5	16.9±1.13	0.7567

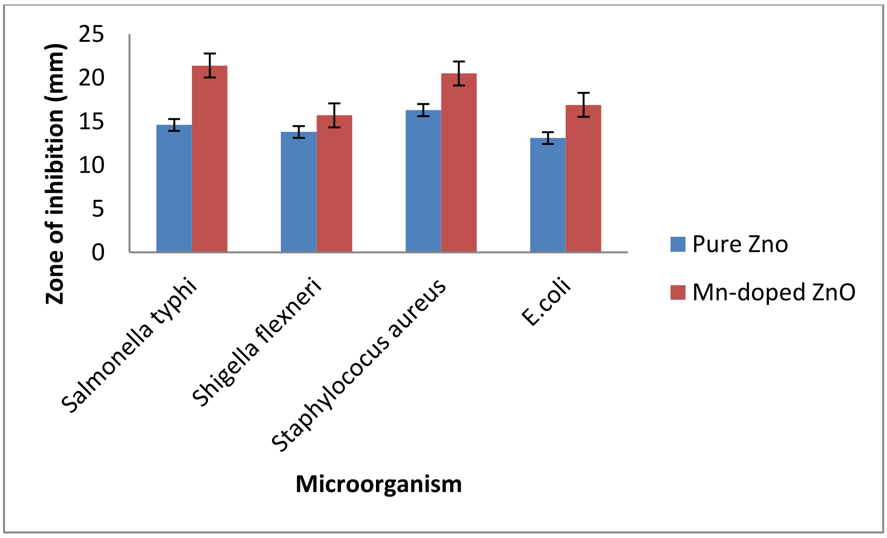

Fig.6.Antimicrobial activity error bar with standard error

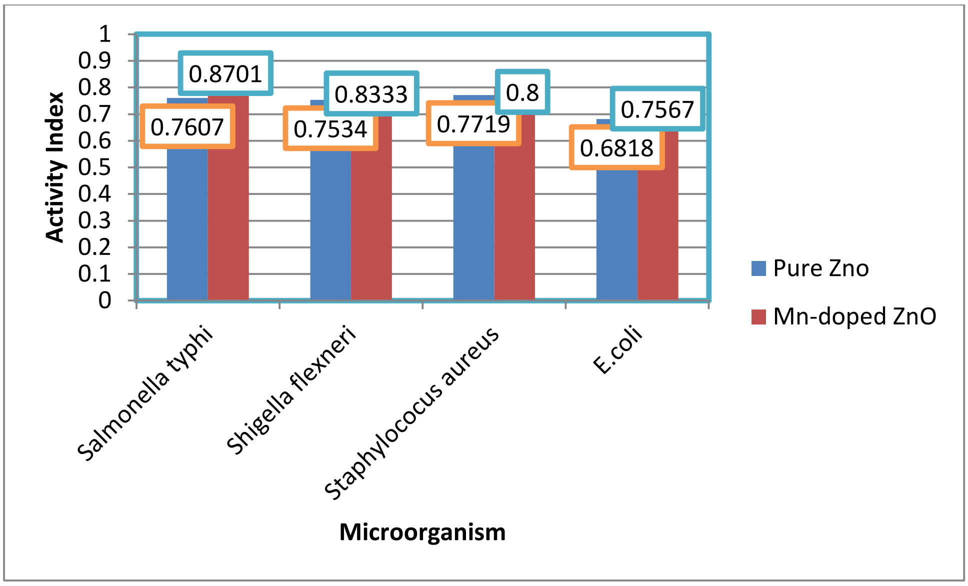

Fig. 7: Activity index bar plot for pure ZnO and Mn-doped ZnO nanoparticles.

IV. CONCLUSION

Manganese-doped ZnO nanoparticles were prepared by aqueous chemical process using the sequential reagent addition method. ZnO nanoparticles were successfully produced using an aqueous chemical process with crystallite sizes ranging from 32 to 46 nm on average. It was investigated how the structural and optical characteristics were affected by different calcination temperatures. The XRD data showed that both pure and Mn-doped ZnO (5 mol%) had pure wurtzite ZnO phase with good crystallinity. The other aspects, including pharmacokinetic studies, immunogenicity, metabolic destiny, and effectiveness, should be thoroughly evaluated before being used commercially. Strong antibacterial activity against *Salmonella typhi*, *E. coli*, Staphylococcus aureus, and *Shigellaflexneri* was shown for both pure and doped ZnO NPs. The maximum activity was found in Mn-doped ZnO (5 mol%.) It was shown that Mn-doped ZnO NPs effectively suppressed the growth of *Shigellaflexneri*, *Salmonella typhi*, *E. coli*, and *Staphylococcus aureus*. These encouraging findings demonstrate the range of biological uses for Mn-doped ZnO NPs. In the future, the doped ZnO nanoparticles will be helpful in treating hyperthermia and wound healing.

Acknowledgements
The authors are thankful to research center of Nehru Gram Bharati (Deemed to be University), Jamunipur, Prayagraj for research work.

Data Availability
The data will be made available on request.

Conflict of Interest
The authors declare no conflicts of interest.

Funding Source
None.

Authors' Contributions
Author -1: Formal analysis; investigation; methodology, performed the experiments and writing—original draft.
Author -2: Conceptualization; supervision.
Author -3: Formal analysis; software.
Author -4: Formal analysis; investigation
Author -5: Software; writing, review and editing

References

[1]. Abou El-Nour, K.M., Eftaiha, A.A., Al-Warthan, A. and Ammar, R.A.[2010] "Synthesis and applications of silver nanoparticles" Arabian journal of chemistry, Vol.3,No.3, pp.135-140.

[2]. Nirmala J.N.S., Sagayaraj, P.[2012] "The influence of capping by TGA and PVP in modifying the structural, morphological, optical and thermal properties of ZnS nanoparticles"ApplSci ResVol.4,No.2, pp.1079–90.

[3]. Alabi, A.B., Coppede, N., Vilani, M., Calestani, D., Zappetini, A., and Babalola, O.[2013] “Photocatalytic activity of nanostructuredcopper (II) oxide particles” Ife J Sci ,Vol.15,No.2,pp.409–14.

[4]. Rao,C.N.R. and Rao G.V.S.[1974] “Transition metal oxide, crystal chemistryphase transition and related aspects”, NSRDS-NBS 49.Washington DC: U.S. Government Printing Office

[5]. Mark T.G., Zheng H.L.,[2013] “Thin-film metal oxides in organic semiconductor devices: their electronic structures, workfunctions and interfaces.” NPG Asia Mater 2013;5:e55, http://dx.doi.org/10.1038/am.2013.29.

[6]. Li, D., Hu, J., Fan, F., Bai, S., Luo, R., Chen, A.,[2012] “Quantum-sized ZnO nanoparticles synthesized in aqueous medium for toxicgases detection.” J Alloys Compd Vol.539.,pp. 205–9.

[7]. Rajeswari, Y.N., Srinivasan, R ., Chandra, B.A.,[2009] “Multi-capping agents in size confinement of ZnO nanostructured particles”Opt Mater,Vol.31, pp.1570–4.

[8]. Kumbhakar, P., Singh, D., Tiwary, C.S., Mitra, A.K.[2008]“Chemical synthesis and visible photoluminescence emission frommonodispersedZnO nanoparticles” Chalcogenide Lett., Vol.5,No.12, pp.387–94.

[9]. Al-Heniti,S., Badran R.I, Umar. A, Al-Ghamdi, A., Kim, S.H,Al-Marzouki. F,.[2011]“Temperature dependant structural andelectrical properties of ZnO nanowire networks’ J NanosciNanotechnol,Vol.11, pp.1–7.

[10]. Wang, Z.H., Geng, D.Y., Han, Z., Zhang, Z.D.[2009] “Characterization and optical properties of ZnO nanoparticles obtained byoxidation of Zn nanoparticles.” Mater Lett Vol.63, pp.2533–5.

[11]. Samuel, S.M., Bose, L., George, K.C.,[2009]”Optical properties of ZnONanoparticles” SB Acad Rev;Vol.1,No.2.,pp.57–65.

[12]. Karami, H., Fakoori ,E., [2011] “Synthesis and characterization of ZnOnanorods based on a new gel pyrolysis method” J Nanomaterhttp://dx.doi.org/10.1155/2011/628203 [Article ID 628203; pp. 11].

[13]. Xudong, W., Jinhui, S., Zhong, L.W.[2007]“Nanowire and nanobeltarrays of zinc oxide from synthesis to properties and tonovel devices.” J Mater Chem ,Vol.17, No.7, pp.11–20.

[14]. Lupan, O., Pauporte, T., Chow, L., Viana, B., Pelle. F, Ono LK,[2010] “Effects of annealing on properties of ZnO thin films prepared by electrochemical deposition in chloride medium” ApplSurfSci Vol.256, pp.1895–907.

[15]. Chen, R., Zou, C., Yan, X., Alyamani, A., Gao, W., [2011] “Growth mechanism of ZnO nanostructures in wet-oxidation process”Thin Solid Films, Vol.519.pp.1837–44.

[16]. Ma, Y., Wang, W.L., Liao, K.J., Kong, C.Y.,[2002] “Study on sensitivity of nano-grain ZnO gas sensors” J Wide Bandgap MaterVol.10.,pp.113–20.

[17]. Ali, A.A., Azam, I.Z., Seyed, M.M, Mohammad, M.A.,[2010]“Photocatalytic activity of ZnO nanoparticles prepared via submerged arc discharge method.” ApplPhys A,Vol.100pp.1097–102.

[18]. Waldo, J.E.B., Martijn, M.W., Martijn, K., Xiaoniu, Y. Rene AJJ.[2005]“Hybrid zinc oxide conjugated polymer bulk heterojunctionsolar cells’ J PhysChem B.Vol.109.pp.9505–16.

[19]. Pandey, P., Singh, N., Haque, F.Z.,[2013] “Development and optical study of hexagonal multi-linked ZnO micro-rods grown using hexamine as capping agent” Optik.Vol.124 pp.1188–2119.

[20]. Singh, A.K., Viswanath, V. Janu, V.C.,[2009] “Synthesis, effect of capping agents, structural, optical and photoluminescence properties of ZnO nanoparticles” J LuminVol.129.,pp.874–8.

[21]. Das, R., & Sarkar, S. [2015] “Determination of intrinsic strain in poly (vinylpyrrolidone)-capped silver nano-hexapod using X-ray diffraction technique” Current Science, pp.775-778.

[22]. Sundaram, P. S., Sangeetha, T., Rajakarthihan, S., Vijayalaksmi, R., Elangovan, A., &Arivazhagan, G. [2020] “XRD structural studies on cobalt doped zinc oxide nanoparticles synthesized by coprecipitation method” Williamson-Hall and size-strain plot approaches” PhysicaB:Condensed Matter, Vol.*595*, 412342.

[23]. Mustapha, S., Ndamitso, M. M., Abdulkareem, A. S., Tijani, J. O., Shuaib, D. T., Mohammed, A. K., &Sumaila, A. [2019] “Comparative study of crystallite size using Williamson-Hall and Debye-Scherrer plots for ZnO nanoparticles’ Advances in Natural Sciences *Nanoscience and Nanotechnology*, *10*(4), 045013.

[24]. Nath, D., Singh, F., & Das, R. [2020]. “X-ray diffraction analysis by Williamson-Hall, Halder-Wagner and size-strain plot methods of CdSe nanoparticles-a comparative study” Materials Chemistry and Physics, Vol.239, 122021.

[25]. Nwaokafor, P., Okeoma, K. B., Echendu, O. K., Ohajianya, A. C., &Egbo, K. O. [2021] “X-ray diffraction analysis of a class of AlMgCu alloy using williamson–hall and scherrer methods” Metallography, Microstructure, and Analysis., Vol.10.,pp.727-735.

[26]. Wang, N., Yang, Y., & Yang, G. [2011] “Great blue-shift of luminescence of ZnO nanoparticle array constructed from ZnO quantum dots” Nanoscale research letters, Vol., 6, pp.1-6.

[27]. Zak, A. K., Majid, W. A., Abrishami, M. E., &Yousefi, R. [2011] “X-ray analysis of ZnO nanoparticles by Williamson–Hall and size–strain plot methods” Solid State Sciences,Vol.13,No.1,pp.251-256.

[28]. Li, D., Hu, J., Fan, F., Bai, S., Luo, R., Chen, A., & Liu, C. C. [2012] “Quantum-sized ZnO nanoparticles synthesized in aqueous medium for toxic gases detection “Journal of alloys and compounds, Vol. 539,pp.205-209.

[29]. Rao, K. V. S., Lavédrine, B., & Boule, P. [2003] “Influence of metallic species on TiO2 for the photocatalytic degradation of dyes and dye intermediates” Journal of Photochemistry and Photobiology A: Chemistry, Vol.154,No.2-3,pp. 189-193.

[30]. Raghupathi, K. R., Koodali, R. T., & Manna, A. C. [2011] “Size-dependent bacterial growth inhibition and mechanism of antibacterial activity of zinc oxide nanoparticles” Langmuir., Vol.27.,No.7.,pp.4020-4028.

[31]. Thiel, J., Pakstis, L., Buzby, S., Raffi, M., Ni, C., Pochan, D. E., & Shah, S. I. [2007] “Antibacterial properties of silver-doped titania” Small, Vol.3,No.5.,pp.799-803.

[32]. Raghupathi, K. R., Koodali, R. T., & Manna, A. C. [2011] “Size-dependent bacterial growth inhibition and mechanism of antibacterial activity of zinc oxide nanoparticles” Langmuir, Vol.27,No.,7,pp. 4020-4028.

[33]. Li, W. R., Xie, X. B., Shi, Q. S., Zeng, H. Y., Ou-Yang, Y. S., & Chen, Y. B. [2010] “Antibacterial activity and mechanism of silver nanoparticles on *Escherichia coli*” Applied microbiology and biotechnology, Vol.85,pp.1115-1122.

[34]. Thiel, J., Pakstis, L., Buzby, S., Raffi, M., Ni, C., Pochan, D. E., & Shah, S. I. [2007]. Antibacterial properties of silver-doped titania. Small, Vol.3.,No.5, pp.799-803.

[35]. Djokić, S. S., & Burrell, R. E. [1998] “Behavior of silver in physiological solutions.”Journal of the Electrochemical Society, Vol.145,No.5,pp.1426.

[36]. Matsumura,Y., Yoshikata, K., Kunisaki, S. I., &Tsuchido, T. [2003]. “Mode of bactericidal action of silver zeolite and its comparison with that of silver nitrate” Applied and environmental microbiology, Vol.*69*.,No.7, pp.4278-4281.